PAPER

Development of poly (1,8 octanediol-co-citrate) and poly (acrylic acid) nanofibrous scaffolds for wound healing applications

To cite this article: Allison Goins *et al* 2018 *Biomed. Mater.* **13** 015002

Biomedical Materials

PAPER

Development of poly (1,8 octanediol-co-citrate) and poly (acrylic acid) nanofibrous scaffolds for wound healing applications

Allison Goins[1,2], **Vidhya Ramaswamy**[1], **Elliott Dirr**[3], **Krista Dulany**[1], **Sean Irby**[1], **Antonio Webb**[1,3] and **Josephine Allen**[1,2,3]

[1] University of Florida, Department of Materials Science and Engineering, 100 Rhines Hall, PO Box 116400, Gainesville, FL 32611, United States of America
[2] University of Florida, Institute for Cell and Tissue Science and Engineering, 300 Weil Hall, PO Box 116550, Gainesville, FL 32611, United States of America
[3] University of Florida, J. Crayton Pruitt Family Department of Biomedical Engineering, 1275 Center Drive, Biomedical Science Building JG-56, PO Box 116131, Gainesville, FL 32611, United States of America

E-mail: jallen@mse.ufl.edu

RECEIVED
23 January 2017

REVISED
30 June 2017

ACCEPTED FOR PUBLICATION
4 August 2017

PUBLISHED
26 October 2017

Keywords: wound healing, fibroblasts, electrospinning, nanofibrous scaffold

Abstract

Wound care is one of the leading health care problems in the United States costing billions of dollars yearly. Annually, millions of acute wounds occur due to surgical procedures or traumas such as burns and abrasions, and these wounds can become non-healing due to bacterial infection or underlying pathologies. Current wound care treatments include the use of bioinert constructs combined with topical administration of anti-bacterial agents and growth factors. However, there is a growing need for the development of bioactive wound dressing materials that are able to promote wound healing and the regeneration of healthy tissue. In this work, we evaluate and report the use of a novel electrospun polymeric scaffold consisting of poly (1,8 octanediol-co-citrate) and poly (acrylic acid) for wound healing applications. The scaffold exhibits intrinsic antibacterial activity, hydrogel-like water uptake abilities, and the ability to deliver physiologically relevant concentrations of growth factor. Additionally, the scaffold shows antibacterial function when tested with bacteria relevant to wound healing applications. Biological characterization of the electrospun scaffold shows excellent cellular adhesion, low cytotoxicity, and enhanced proliferation of skin fibroblasts. This work has potential towards the development of novel bioactive scaffolds for prevention of bacterial infiltration into the wound bed and enhanced healing.

1. Introduction

With approximately 70 million surgical procedures performed each year globally, there is a critical need for post-surgical wound care that promotes healing and prevents infection [1]. According to the National Healthcare Safety Network's national and state healthcare-associated infections progress report from 2016, approximately 1% of surgeries performed in the United States result in a surgical site infection [2]. In addition to the number of acute wounds created by surgical procedures they can also be produced by traumas, abrasions, or superficial burns. Many of these wounds that remain open subsequent to surgical intervention risk infection and can become non-healing due to the infiltration of bacteria or underlying comorbidities. For the purposes of this study, we focused on dressings for open wounds that may include those that develop a non-healing pathology due to bacterial infection. Current treatment methods utilize passive constructs combined with topical administration of anti-bacterial agents and growth factors to prevent infection and promote healing [3]. This treatment plan is limited because it relies heavily on patient compliance and introduces opportunities for infection. More specifically, patients must frequently change the wound dressings which can be very painful, and each dressing change exposes the wound to bacteria. Engineered bioactive scaffolds offer an attractive alternative for traditional wound dressings. An anti-bacterial scaffold that prevents infection and can promote tissue regeneration via drug delivery

would be a suitable alternative. In this work, we fabricated and characterized an electrospun material system towards the development of an inexpensive readily available scaffold that can reduce the number of dressing changes necessary, prevent bacterial infiltration, and promote tissue regeneration. In order to fabricate a scaffold that meets the clinical requirements for an open wound dressing the material must be able to: (1) conform to the wound bed, (2) uptake wound exudate, (3) have antibacterial properties, (4) the ability to deliver regeneration promoting factors directly to the wound bed, and (5) made from biocompatible and biodegradable materials. Additionally, a scaffold fabricated from low cost materials with an easily scalable process would be ideal to ensure its low cost and ready availability. Towards achieving this goal, this study was designed to show feasibility of an electrospun scaffold made from biodegradable biocompatible synthetic polymers with inherent antibacterial character and loaded with a physiologically relevant growth factor to meet these design costraints.

Many scaffold fabrication techniques have been developed that provide controlled scaffold architecture, and are able to mimic structures found *in vivo*. Electrospinning, a technique that is particularly ideal for wound healing applications creates highly porous nanofibrous structures. Electrospun nanofibers mimic the geometry of native extracellular matrix (ECM) found in the dermal layer of skin and can potentially provide structural cues to cells which are essential for enhanced tissue regeneration [4, 5]. Recent reports have shown that electrospun scaffolds for wound healing applications can be fabricated from both natural materials such as: cellulose derivatives (chitin and chitosan) [6–8] and gelatin [5] or synthetic materials such as: poly (ε-caprolactone) (PCL) [5], poly (lactic-co-glycolic acid) (PLGA) [9], poly (vinyl alcohol) [7, 10], poly (vinylpyrrolidone) [10], and poly (acrylic acid) (PAA) [10]. Synthetic materials are more advantageous than natural materials for wound healing applications because they are readily available, tailorable, and inexpensive to produce on a commercial scale.

This study reports the potential of a novel electrospun polymeric scaffold consisting of a blend of poly (1,8 octanediol-co-citrate) (POC) and PAA as a candidate material system for wound healing applications. POC, belonging to the family poly diol citrate elastomers, was chosen because of its reported biocompatibility and hemocompatibility properties, and its ability to support angiogenesis [11–13]. In addition to the biocompatibility of POC, it has been shown to have inherent antibacterial activity [14, 15]. PAA is also a biocompatible material that has been used in hydrogel applications. Due to the enhanced moisture retention necessary for tissue rehydration and regrowth, PAA was selected to act as a hydrogel-like component in this scaffold [10, 16]. Towards the goal of regeneration promoting scaffolds, bioactive wound dressings from synthetic materials are currently being developed to deliver growth factors that promote tissue regrowth and angiogenesis in the wound bed [9, 17]. Designing a scaffold to meet all of these requirements is advantageous in the development of a new generation of bioactive wound dressing technology. In this study a candidate growth factor, platelet derived growth factor (PDGF-$\beta\beta$) was selected as it is present in the wound bed during regeneration, and has been shown to promote wound healing and angiogenesis [18]. This study investigates the potential of this material system to meet a set of design requirements that it is believed would allow the system to meet the clinical requirements for wound healing applications. Specifically, in this study, we optimized the electrospinning parameters to meet the design constraints by characterizing the electrospun nanofiber structure, assessing the antibacterial activity, evaluating the growth factor delivery potential, as well as analyzing dermal fibroblast cell viability and proliferation on the scaffolds. This work serves as a foundation for future studies to develop a material system that can meet the design constraints at the level needed to meet the clinical requirements.

2. Materials and methods

2.1. Materials

POC pre-polymer was synthesized as previously reported [19]. Briefly, equimolar amounts of 1,8-octanediol (Sigma Aldrich, St. Louis, MO) and citric acid (Sigma Aldrich, St. Louis, MO) were heated to 165 °C until molten, upon which the polycondensation reaction was carried out at 140 °C for an hour and a half. The pre-polymer solution was then purified to remove unreacted monomers via dissolution in ethanol followed by precipitation in water and lyophilization (Labcono Freezone 2.5, Kansas City, MO). The pre-polymer was then reconstituted at 10 wt.% in ethanol for electrospinning. PAA (MW ~ 450 000) (Sigma Aldrich, St. Louis, MO) was dissolved in ethanol at 10 wt.% at room temperature.

2.2. Fabrication of scaffolds

Varying relative weight ratios of the 10 wt.% POC and PAA solutions: 80:20, 70:30, 60:40, 50:50, 40:60, 30:70, 20:80, 0:100 were mixed under magnetic stirring for electrospinning. The polymer solutions were fed through a 25 G needle at 2 ml h^{-1} with a syringe pump (Chemyx Fusion 100, Stafford, TX), and collected on an aluminum substrate. The working distance was 15 cm and a voltage potential of 14–22 kV was produced with a high voltage source (Gamma High Voltage ES 30, Ormond Beach. FL). After electrospinning, the scaffolds were crosslinked at 80 °C for 1 d followed by 100 °C for 2 d.

2.3. Morphological and chemical characterization

Analysis of fiber morphology of the electrospun POC:PAA scaffolds at all weight ratios was performed using scanning electron microscopy (SEM) (PhenomWorld ProX, Eindhoven, Netherlands). Samples were cut into sections and mounted onto 15 mm diameter aluminum stubs, sputter coated with gold–palladium, then subsequently imaged. Fiber diameters were determined from the SEM images, measuring 20 randomly selected fibers on 5 total images at 10 000× magnification [10]. Fiber diameter measurements were made using ImageJ software (National Institutes of Health, Bethesda, MD).

Chemical analysis of the electrospun scaffolds was performed using attenuated total reflectance Fourier transformation infrared spectroscopy (ATR-FTIR). ATR-FTIR spectra were obtained for each of the samples using the Nicolet 6700 FTIR Spectrometer (ThermoFisher Scientific, Waltman, MA) and a diamond tip window. The relative intensity was measured over a range of 600–4000 cm^{-1} for each sample and a total of 32 scans were used with a resolution of 4 cm^{-1}.

Contact angle measurements were performed on a custom-made goniometer. Thin films were prepared by solution casting the pre-polymer mixes into glass petri dishes and crosslinking at 80 °C for 1 d and 100 °C for 2 d. Subsequent to crosslinking, the films were hydrated in nanopure water and removed from the substrate. The films were then frozen at −80 °C for an hour then lyophilized overnight. Deionized (DI) water (5 μl) was dropped onto the thin films, and the contact angle was measured after droplet equilibration on the film.

Water uptake capacity of the scaffolds was also evaluated. In this assessment, the electrospun nanofibrous scaffolds were crosslinked as described. The weight of the scaffold was measured, W_i; then the scaffolds were placed in 1 ml of DI water. The scaffolds were allowed to equilibrate overnight in water then removed from the DI water. Subsequently, the hydrated weight was measured, W_h. The following equation was then used to calculate percent water uptake for the scaffolds, equation (1) [20]:

$$\%\ \text{water uptake} = \frac{W_h - W_i}{W_i} \times 100. \quad (1)$$

The porosity of the scaffolds was measured using a modified Archimedes' principle [21]. A density bottle was filled with ethanol and the temperature of the ethanol was equilibrated to 37 °C in a water bath. Prior to immersion in the ethanol, the weight of the scaffold was recorded, W_s. Once the solution temperature reached approximately 37 °C the weight of the bottle and ethanol was recorded, W_1. The scaffold was then immersed in the density bottle and the air bubbles in the scaffold's pores were removed under vacuum; the ethanol removed during the degassing process was replaced and the solution temperature was equilibrated again to 37 °C. The weight of the bottle with the scaffold was measured, W_2, then the scaffold was removed from the density bottle and the weight was recorded, W_3. To calculate porosity, ε (equation (4)) the following parameters were calculated: volume of the scaffold pores, V_p (equation (2)) and the volume of the skeleton, V_s (equation (3)). The density of ethanol at 37 °C, ρ_e was used to calculate each of the parameters.

$$V_p = \frac{(W_2 - W_3 - W_s)}{\rho_e}, \quad (2)$$

$$V_s = \frac{(W_1 - W_2 + W_s)}{\rho_e}, \quad (3)$$

$$\varepsilon = \frac{V_p}{V_p + V_s}. \quad (4)$$

2.4. Antibacterial assessment of scaffold

POC:PAA scaffolds were cut into discs 9.5 mm in diameter and approximately 0.5 mm thick, washed twice in PBS, once in water, lyophilized overnight, then gas sterilized with ethylene oxide (Anaprolene AN741 Vernon Hills, IL). Antibacterial assessments were performed with *Escherichia coli (E. coli)* strain # 25922 and *Staphylococcus aureus (S. aureus)* strain # 25923 (ATCC, Manassas, VA). Bacteria were inoculated into nutrient rich culture medium (broth) followed by a 12 h growth incubation. The bacteria in culture after 12 h represents the initial bacteria population from which subsequent growth was assessed. An aliquot of the initial bacterial culture was added to wells containing sterile POC:PAA scaffolds. After 12 and 36 h the optical density of the broth at 600 nm was measured to assess bacterial growth with an increase in optical density correlating with an increase in broth turbidity and thus an increase in bacterial growth. Optical density was obtained using the Synergy H1 microplate spectrophotometer (BioTek Instruments, Winooski, VT).

2.5. Growth factor release kinetics from POC:PAA scaffolds

The electrospun POC:PAA scaffolds were cut into 6.35 mm diameter and approximately 0.5 mm thick discs, washed twice in PBS, once in water, then lyophilized overnight. Following lyophilization, the scaffolds were incubated in a solution of excess PDGF-$\beta\beta$ for growth factor adsorption. A 1 μg ml^{-1} solution of PDGF-$\beta\beta$ (R&D Systems, Minneapolis, MN) in PBS was prepared and scaffolds were incubated overnight. Scaffolds containing loaded growth factors were freeze dried once again. To initiate the release of bound growth factors, the scaffolds were placed in microcentrifuge tubes with 1 ml PBS. At various time points over 7 d, the entire 1 ml of PBS solution containing released growth factor was collected and replaced. The releasate from each time point was quantitatively assayed via enzyme-linked immunosorbent assay (ELISA) for total PDGF-$\beta\beta$ via Human PDGF-$\beta\beta$ Quantikine ELISA kit (R&D Systems, Minneapolis,

MN). The cumulative release of the growth factor with respect to time was reported.

The concentration of growth factor loaded into the POC:PAA scaffolds was quantified via the NanoOrange Protein Quantification Kit (ThermoFisher Scientific, Waltman, MA). Subsequent to incubation of the scaffolds in the solution of 1 μg ml^{-1} PDGF-$\beta\beta$ as described above, the supernatant was collected and assayed. The supernatant which contained the remaining protein that was unbound was diluted to 2% with the NanoOrange® working solution as per the kit instructions and then incubated at 90 °C for 10 min to unfold the protein and allow for binding of the fluorophore. The fluorescence was measured at an excitation wavelength of 460 nm and an emission wavelength of 590 nm on the Synergy H1 plate reader. A standard curve was prepared with bovine serum albumin and used to extrapolate the protein concentration in the supernatant.

2.6. Cell culture

All biocompatibility assays were performed using Detroit 551 (D551) (ATCC, Manassas, VA), a human skin fibroblasts cell line. D551 growth media was made using Eagle's minimum essential medium (EMEM) supplemented with 10% fetal bovine serum (FBS). D551 cells between passages 3–5 were cultured in an incubator held at 37 °C, 5% CO_2 and constant humidity. For all cellular assays, scaffolds were cut into 6.35 mm diameter and approximately 0.5 mm thick discs.

2.7. Biological activity of released growth factor

D551 cells were plated on the bottom surface of a Transwell™ culture plate (Corning, Corning, NY) and grown to confluency in D551 complete growth media. POC:PAA scaffolds were incubated overnight in a 1 μg ml^{-1} solution of PDGF-$\beta\beta$ or saline followed by lyophilization. Prior to the start of the experiment, cells were synchronized by serum starvation using EMEM supplemented with 1% FBS for 18 h. Post starvation, a 'wound' was created using a P-200 pipette tip to scrape away an area of cells within the monolayer followed by rinsing with PBS to remove the detached cells. Initial wound size was imaged using an inverted TE2000U microscope (Nikon, Tokyo, Japan). Growth factor-loaded or saline loaded scaffolds were placed into the upper chamber of the Transwell™ plate, and the well filled with low serum growth media. Migration after 15 h was assessed optically by imaging the cell monolayer using an inverted microscope, and the change in wound area analyzed using ImageJ.

2.8. Cell adhesion to POC:PAA scaffold

To assess the adhesion of cells on the scaffolds, POC:PAA scaffolds were seeded with 40 000 D551 cells. After overnight culture in D551 complete growth media, the cell seeded scaffolds were rinsed twice with PBS then fixed with 2% glutaraldehyde in PBS for 30 min at room temperature. Cell seeded scaffolds were then dehydrated in a graded series of ethanol, frozen at −80 °C and lyophilized overnight before being mounted and sputter coated with gold palladium for SEM analysis. The cellular attachment was visualized via SEM.

2.9. Cytotoxicity of POC:PAA scaffold

Cytotoxicity of the POC:PAA scaffolds was measured using a lactate dehydrogenase (LDH) cytotoxicity assay kit (ThermoFisher Scientific, Waltman MA). The cytotoxicity of the scaffold was assessed by quantifying the release of soluble LDH, an enzyme found when the cell membrane is damaged, an indicator of cell death. Briefly, 50 000 D551 cells were seeded onto the POC:PAA scaffolds and cultured for 2 d. At 2 d the media was transferred into a 96 well plate and assayed for LDH concentration following standard kit instructions and utilizing a Synergy H1 microplate reader. For reference, in a subset of samples, the maximum degree of cell lysis, maximum relative LDH concentration was obtained by treating cells grown on the test surfaces with lysis buffer. The data reported are relative to maximum LDH concentration or complete cell death.

2.10. Cell proliferation on POC:PAA scaffold

Cell proliferation was assessed using a (3-(4,5-dimethylthiazol-2-yl)-2, 5-diphenyl tetrazolium bromide) (MTT) assay, following standard kit instructions (MTT Cell Proliferation Assay Kit, Trevigen, Gaithersburg, MD) and analyzed on a Synergy H1 microplate reader. Briefly, POC:PAA scaffolds cut into ¼″ discs were placed in 24-well ultra-low attachment plate then 10 000 D551 cells were seeded onto each scaffold. The cells were cultured over 7 d to assess proliferation on the scaffolds over time. At pre-defined time points MTT reagent was added to the well and incubated for 4 h, and then detergent was added to solubilize the crystals produced. The media were collected and the absorbance measured. A standard curve was used to extrapolate cell number, and the absorbance of solubilized formazan crystals was plotted versus cell number. An increase in cell number was correlated with increased proliferation.

2.11. Statistical analysis

All numerical data are reported as an average ± standard deviation. Statistical significance was determined using one-way analysis of variance test with Fisher's LSD as the post hoc analysis. A p-value of <0.05 was used to confirm statistical significance.

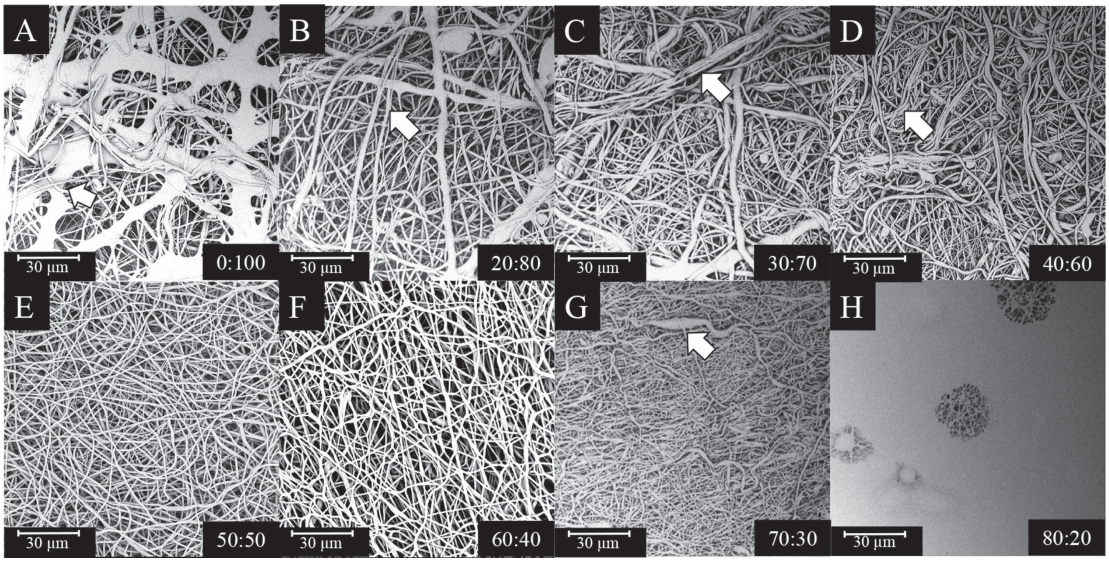

Figure 1. Representative SEM images of electrospun POC: PAA fibrous scaffolds at varying weight ratios from 0%–80% POC and 100%–20% PAA. Panel A is a fibrous scaffold composed of 100% PAA with no POC, while panels B–H are fibrous scaffolds composed of increasing concentrations of POC from 20%–80% and correspondingly decreasing concentrations of PAA from 80%–20%, respectively. White arrows above indicate areas where there is coalescing of the fibers and beading. All images are 2000×.

3. Results

3.1. Morphological and chemical characterization of the scaffolds

Electrospun composite scaffolds of POC and PAA were fabricated at varying weight ratios ranging from 0:100 POC:PAA to 80:20 POC:PAA. We were unable to successfully electrospin the compositions that contained very high concentrations of POC, 90:10 or 100:0. We believe this is because POC is a thermosetting polymer that flows in the pre-polymer stage resulting in fibers that merge and coalesce. We were successful with the remaining POC:PAA ratios therefore, morphological assessment, and fiber distribution measurements for each of the weight ratios was performed through analysis of SEM images. SEM imaging revealed the 0:100 scaffolds had large agglomerates that resembled portions of a film (figure 1(A)). Scaffolds spun from the 20:80, 30:70 and 40:60 weight ratios showed coalescing of the fibers, and the fiber size was non-uniform (figures 1(B)–(D) white arrows). The 70:30 scaffolds showed very densely packed fibers and there was some beading (white arrows) (figure 1(G)). The 80:20 POC:PAA ratio did not lead to a nanofibrous network but rather, the fibers coalesced forming a polymeric thin film (white arrows) (figure 1(H)). In contrast to other weight ratios tested, scaffolds that contained POC:PAA ratios of 50:50 and 60:40 produced the most uniform, beadless microporous structures and were selected to be used for further studies (figures 1(E), (F)). Digital images of the scaffolds show the flexible nanofibrous mat in the hydrated and dehydrated state (figure 2). The average fiber diameter ranged from 200–1800 nm for POC: PAA scaffolds at a ratio of 50:50. In contrast, the average fiber diameter ranged from 200–1200 nm for POC:PAA scaffolds at a ratio of 60:40 (figure 3). On average POC:PAA scaffolds fabricated at a ratio of 50:50 had larger fibers than the 60:40 scaffolds (table 1). The porosity of the two scaffolds was measured; the 50:50 POC: PAA scaffolds were 88.40% ± 3.91% porous and the 60:40 POC:PAA were 83.75% ± 5.57% porous with no statistical difference between the two polymer composite ratios (table 1).

The hydrophilic character of the polymer blend at the selected compositions was measured via contact angle. The films with the 50:50 composition had a contact angle of 53.21° ± 3.21° which is statistically greater than the contact angle of the films with the 60:40 composition of 47.86° ± 3.52° ($p < 0.05$) (table 1). Similarly water absorption capacity of the 50:50 scaffolds were found to be, 886.65% ± 208.45% which was significantly greater than the 60:40 scaffolds, with an absorption of 504.34 ± 30 ($p < 0.05$) (table 1).

The FTIR spectra for the 60:40 (figure 4(a)) and 50:50 (figure 4(b)). POC:PAA scaffolds crosslinked (solid line) and uncrosslinked (dashed line) was taken. The spectral data revealed for both weight ratios of the uncrosslinked scaffolds, there was a strong broad peak in the range of 3100–3600 cm^{-1}. The presence of the peak comes from the prevalant number of alcohol (O–H) bonds in both the PAA and POC. While this peak is faintly present in the crosslinked spectra it is drastically decreased. The distinct peak around 1600–1700 cm^{-1} indicates the presence of carbon and oxygen bonding. In the crosslinked spectra the peak has a higher intensity indicating an increase in the presence of carbon and oxygen bonding. Similarly the peak from 1000–1300 cm^{-1} indicates bonding

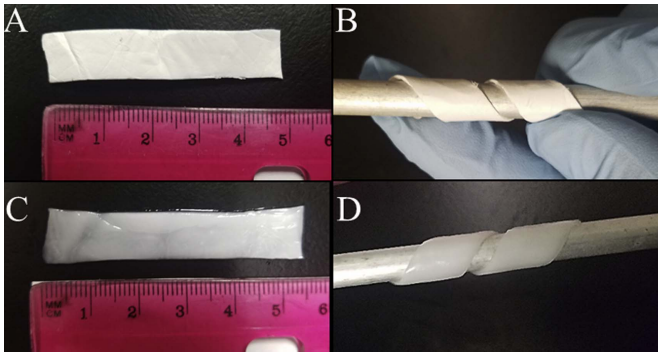

Figure 2. Representative digital images of flexible 60:40 POC:PAA scaffolds in the dehydrated (dry) state (a), (b) and in a fully hydrated state (c), (d).

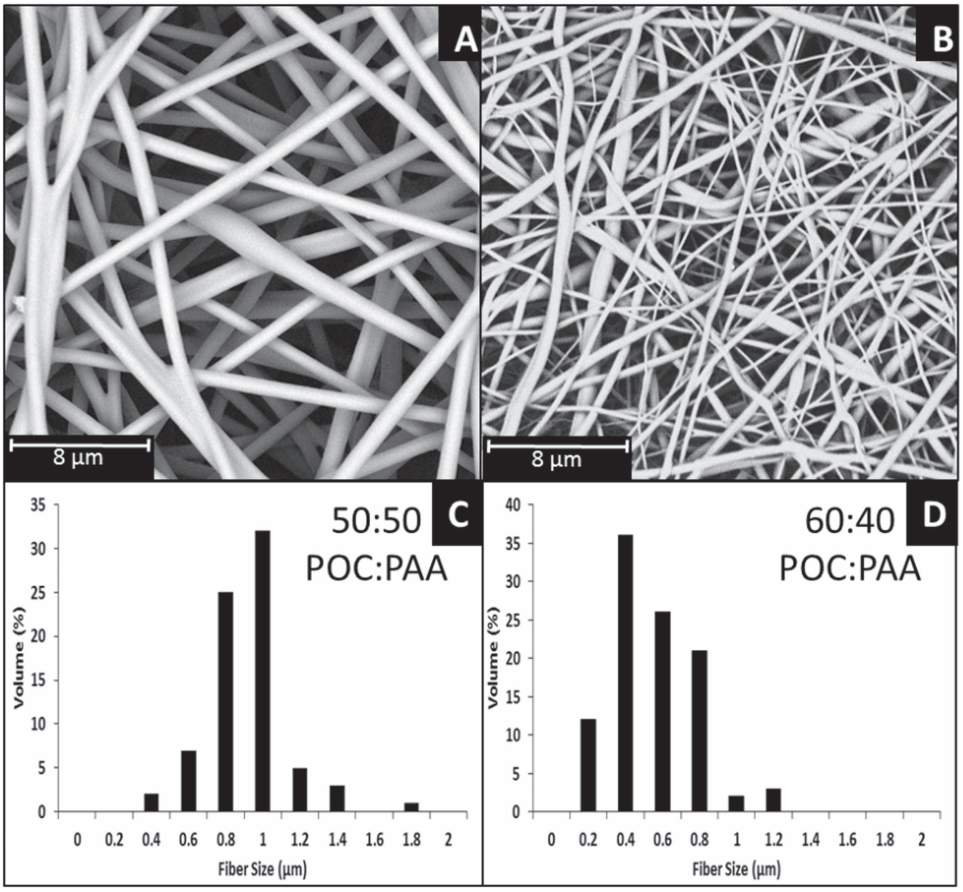

Figure 3. Representative SEM images of 50:50 (a) and 60:40 (b) POC:PAA electrospun scaffolds. Images are 1000×. Histograms representing fiber distribution of the (c) 50:50 and (d) 60:40 POC:PAA electrospun scaffolds ($n = 5$).

Table 1. Morphological and chemical characteristics of the POC:PAA films (contact angle ($n = 3$)) and the electrospun POC:PAA scaffolds (fiber size ($n = 5$), porosity ($n = 5$), and water uptake ($n = 5$)).

Polymer ratio (POC:PAA)	Contact angle (°)	Fiber size (nm)	Porosity (%)	Water uptake (%)
50:50	53.21 ± 3.21	825.8 ± 215.7	88.40 ± 3.91	886.7 ± 208.5
60:40	47.86 ± 3.52	451.2 ± 227.0	83.75 ± 5.57	504.3 ± 30.12

between carbon and oxygen, and the peak has a higher intensity in the crosslinked samples versus the uncrosslinked samples. Based on the hypothesized mechanism of crosslinking, an esterification occurring via condensation reaction the FTIR spectra corroborates this hypothesis with the increased in the presence of carbonyl bonds and decrease in alcohol groups. The crosslinked spectra also have increases in the intensity

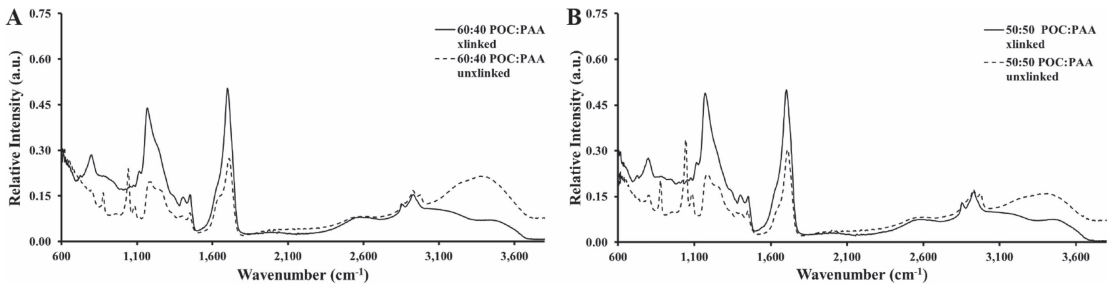

Figure 4. ATR- FTIR spectrum of the crosslinked (solid line) and uncrosslinked (dashed line) 60:40 POC:PAA (a) and the 50:50 POC:PAA (b) electrospun scaffolds.

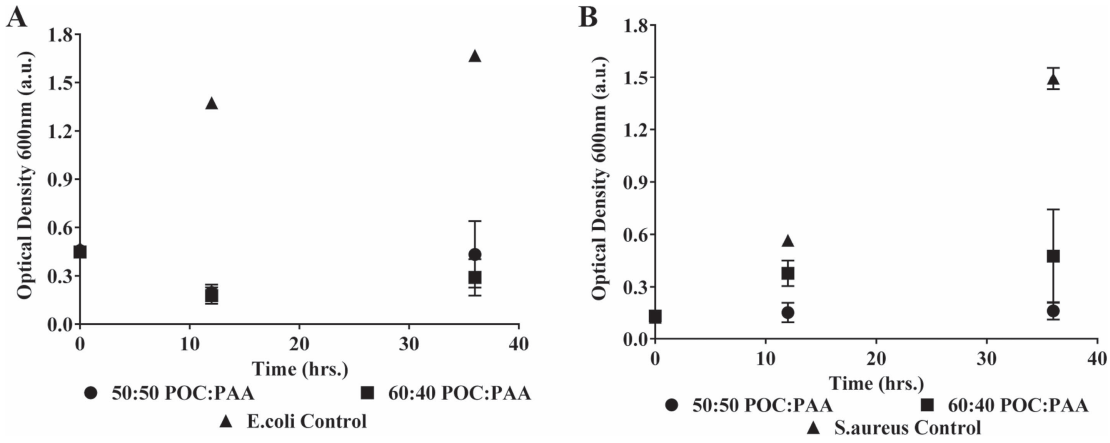

Figure 5. Bacterial growth over 36 h in nutrient rich medium subsequent to incubation with and without 50:50 and 60:40 POC:PAA scaffolds. *E. coli* (a) and *S. aureus* (b) ($n = 3$). Data are reported mean ± SD.

of the peaks at 1200 cm^{-1} which indicate an increase in bonds formed between the carbon and oxygen in the carboxylic acid and ester groups.

3.2. Antibacterial assessment of scaffolds

Antibacterial activity of both weight ratios of POC:PAA scaffolds was assessed with *E. coli* and *S. aureus* via indirect quantification of bacterial growth via optical density measurements at 600 nm. After the 12 h. growth incubation the initial optical density for the *E. coli* and *S. aureus* was 0.476 ± 0.019 and 0.127 ± 0.017 respectively. The 50:50 POC:PAA scaffolds incubated with broth containing *E. coli* had an OD 600 of 0.197 ± 0.049 at 12 h, and 0.434 ± 0.206 at 36 h (figure 5(a)). Comparatively, 50:50 POC:PAA scaffolds incubated with broth containing *S. aureus* had an OD 600 of 0.154 ± 0.056 at 12 h and 0.163 ± 0.050 at 36 h (figure 5(b)). The 60:40 scaffolds that were incubated with *E. coli* had an OD 600 of 0.178 ± 0.051 at 12 h and 0.291 ± 0.113 at 36 h (figure 5(a)). Similarly, 60:40 scaffolds that were incubated with *S. aureus* had an OD 600 of 0.378 ± 0.083 at 12 h and 0.476 ± 0.268 at 36 h (figure 5(b)). For both the 50:50 and 60:40 scaffolds the absorbance (i.e. bacteria density) was statistically lower than their respective *S. aureus* and *E. coli* controls at 12 and 36 h ($p < 0.05$). Overall there was approximately a 1500% increase in bacterial growth in *E. coli* and *S. aureus* over 36 h when cultured in the absence of any scaffolds. Comparatively, there was a 170% and 500% increase in bacterial growth for the 50:50 and 60:40 POC:PAA scaffolds incubated with *S. aureus* respectively, and a 400% and 260% increase in bacterial growth for the 50:50 and 60:40 POC:PAA scaffolds incubated with *E. coli.*

3.3. Growth factor release kinetics of scaffolds

The scaffolds were incubated with PDGF-$\beta\beta$ at a concentration of 1 $\mu g\,ml^{-1}$ to allow for nonspecific adsorption onto the scaffold. Based on the concentration of unbound PDGF-$\beta\beta$, we determined that the 50:50 POC:PAA adsorbed 126.92 ± 0.6 pg mg^{-1} (pg of protein mg^{-1} of scaffold weight) and released 25.38 pg mg^{-1} which represented approximately 38% of the adsorbed protein. While the 60:40 POC:PAA scaffold adsorbed 216.44 ± 0.46 pg mg^{-1}, released 43.29 pg mg^{-1} which represented approximately 57%. The POC:PAA scaffolds loaded with PDGF-$\beta\beta$ experienced an initial burst release within the first 24 h followed by sustained PDGF-$\beta\beta$ release over 7 d. Subsequent to the early burst release, the release rate decreased gradually over 7 d. (figure 6). The data show that the 60:40 POC:PAA scaffolds released statistically more PDGF-$\beta\beta$ than the 50:50 POC:PAA scaffolds.

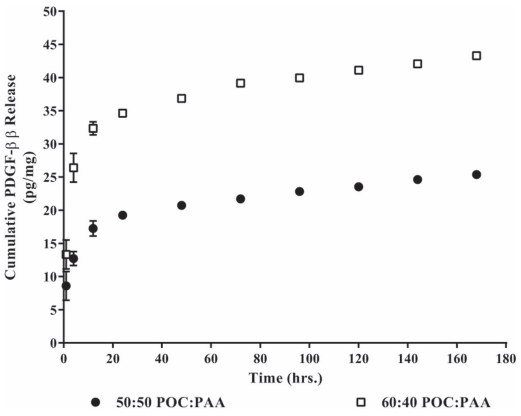

Figure 6. Cumulative PDGF-$\beta\beta$ release from 50:50 and 60:40 POC:PAA scaffolds. Data reported are mean ± SD ($n = 5$).

This was expected due to the statistically higher protein adsorption achieved by the 60:40 POC:PAA scaffolds. The PDGF-$\beta\beta$ loaded scaffolds showed statistically significant release at each time point relative to the $t = 0$ ($p < 0.05$). This indicated for both the 50:50 and 60:40 POC:PAA scaffolds that there was sustained release of PDGF-$\beta\beta$ over 7 d.

3.4. Bioactivity of released growth factor

Biological activity of released PDGF-$\beta\beta$ growth factor was assessed via scratch migration assay ('wound' assay). Migration of Detroit 551 human skin fibroblast cell line was assessed after 15 h of growth factor release from the 50:50 and 60:40 POC:PAA scaffolds. After 15 h the cells incubated with the PDGF-$\beta\beta$ loaded 50:50 and 60:40 scaffolds achieved 88.84% ± 16.97% and 87.25% ± 15.76% 'wound' closure, respectively (figure 7). The negative control scaffolds incubated in saline instead of growth factor, had 34.91% ± 21.51% for the 50:50 scaffolds and 69.27% ± 11.73% for the 60:40 scaffolds 'wound' closure after 15 h. In all case, the cells incubated with electrospun scaffolds loaded with PDGF-$\beta\beta$ showed greater migratory function as evidenced by statistically greater 'wound' closure than the corresponding unsupplemented or saline loaded scaffolds ($p < 0.05$).

3.5. Biocompatibility evaluation of scaffolds

In addition to assessing the structural and chemical compatibility of the scaffold, the biological compatibility was also measured with Detroit 551 human skin fibroblast cell line. Attachment of the cells onto the scaffolds was assessed via SEM imaging after overnight cell attachment. SEM images revealed the fibroblast cells attached and spread on the 50:50 POC:PAA scaffold surface and began to form cellular sheets (figures 8(a), (b)). After 2 d the relative % LDH was 29.01% ± 5.10% and 20.54% ± 1.88% for the 50:50 and 60:40 POC:PAA scaffolds ($p > 0.05$), respectively (figure 9).

Normal cell turnover or normal cell death, as indicated by LDH release from cells cultured on tissue culture polystyrene, was calculated as 15.06% ± 9.34%. There was no statistical significance between the 50:50 or the 60:40 scaffolds and normal cell turnover on tissue culture plastic (TCP) ($p > 0.05$).

In addition to measuring cytotoxicity via LDH concentration, the rate of proliferation and cell viability was measured using an MTT assay. The data revealed after 4 d there was an increase in the population from 10 000 cells to approximately 100 000 cells and 130 000 cells for the 50:50 and 60:40 scaffolds, respectively (figure 10). After 7 d the degree of fibroblast cell proliferation on both scaffolds (50:50 and 60:40) was increased by more than tenfold.

4. Discussion

Electrospun scaffolds offer an attractive option for many tissue engineering applications because they are structurally similar to native ECM and can be synthesized from a wide range of synthetic and natural materials. In addition, they provide an interconnected porous geometry for wound healing allowing for cellular respiration, and high gas permeation to protect the wound from infection and dehydration [22]. Wound dressings are typically inert constructs that protect the wound bed while the tissue regenerates itself. However recent work in the area of wound dressings has moved from passive materials to bioactive scaffolds that aid in the healing process. In this work, we evaluated the potential of a new composite material system consisting of POC and PAA to meet previously outlined clinical requirements to serve as a bioactive wound dressing. Specifically, we characterized the electrospun nanofiber structure in order to show how it mimics the natural ECM and can conform to a wound bed; and we determined the ability of the scaffold to uptake fluids, have antibacterial activity, and deliver a growth factor which helps *in vitro* dermal fibroblast cell viability and proliferation on the scaffolds.

Our initial fabrication of a wide range of POC:PAA compositions revealed large variability in the nanofiber network structure with composition. The compositions with higher concentrations of PAA had fusing or coalescing of fibers, while the compositions with a higher concentration of POC merged to create film-like structures. We found in our scaffold fabrication that there was an optimal balance between POC and PAA polymer ratios, which allowed for the fabrication of a nanofibrous network with uniform fiber geometry and a narrow fiber distribution. A more advantageous structure is possible in both the 50:50 and 60:40 POC:PAA ratios. Given the flexible nature of the scaffolds in both wet and dry state, it is possible that the scaffold can conform to the wound geometry. This has been shown for textiles whereby a direct correlation

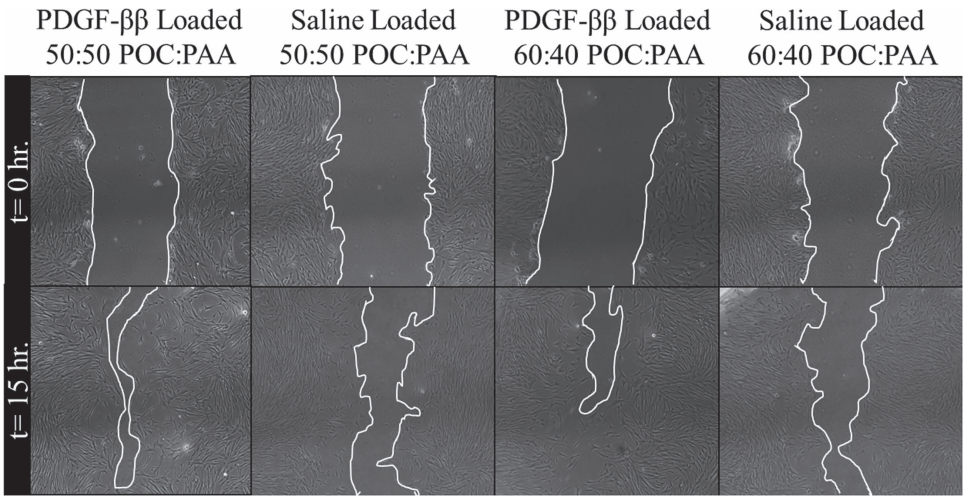

Figure 7. Representative optical images of the D551 cells in the scratch 'wound healing' assay. Each image shows the percent area closure or migration of scratched D551 cells treated with PDGF-$\beta\beta$ loaded 50:50 and 60:40 scaffolds, as well as saline loaded control scaffolds. Data reported are mean ± SD ($n = 5$).

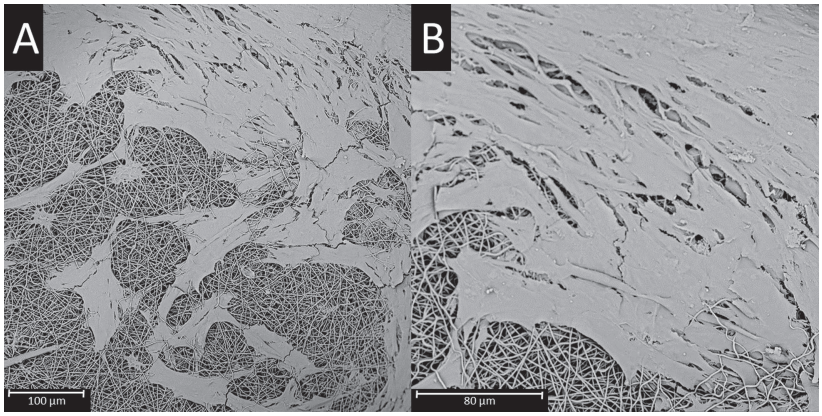

Figure 8. Representative SEM images of D551 cells cultured on 50:50 POC:PAA scaffolds after 24 h of cell attachment, taken at 500× (a) and 1000× (b).

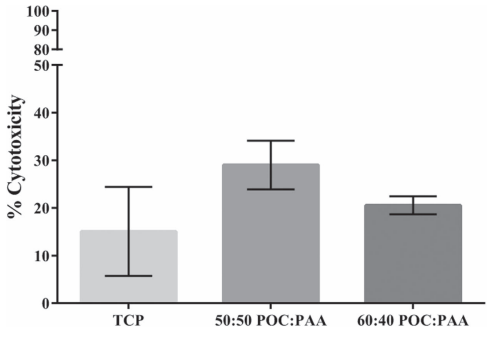

Figure 9. Percent cytotoxicity data extrapolated from LDH concentration in media after D551 cells are cultured for 2 d. Data reported are mean ± SD ($n = 4$).

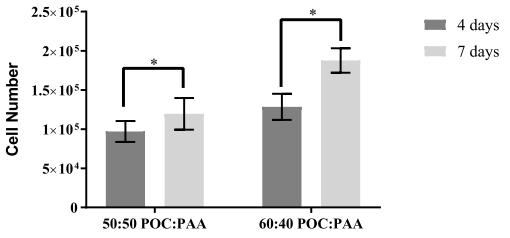

Figure 10. Proliferation results from MTT assay correlating concentration of formazan crystals to cell number for both the 50:50 and 60:40 weight ratios of POC:PAA scaffolds. Data are reported mean ± SD ($n = 4$).

between the fiber diameter and conformability has been shown [22]. Conformability is essential for wound dressings because they must integrate into the irregular geometry of the wound. Electrospun scaffolds with ultra-fine average fiber diameters are more flexible and able to accommodate irregular wound geometries. In addition to conformability, nanofibrous meshes have also been shown to promote hemostasis [22, 23]. Due to the high surface area to volume ratio of electrospun scaffolds there is more surface area for blood components to interact and initiate clot formation, which assists hemostasis in the

wound bed [24]. Likewise fiber diameter has been correlated to cellular adhesion, spreading and proliferation. Kumbar *et al* showed electrospun PLGA scaffolds with fiber diameters between 250 and 1200 nm experienced greater adhesion, spreading and proliferation of dermal fibroblasts compared to scaffolds with fibers less than 250 nm or greater than 1200 nm [25]. Similarly, Chen *et al* showed proliferation and adhesion of NIH 3T3 fibroblasts on electrospun PCL scaffolds were greatest on scaffolds with fibers of 428 nm [26]. The fiber diameter distribution of the POC:PAA scaffolds is within the range identified that can support increased human dermal fibroblast adhesion, spreading, and proliferation. Therefore, we would expect that the POC:PAA electrospun scaffolds that we have fabricated at the 50:50 and 60:40 ratios with the smaller fiber diameters, will be appropriate for contouring to the wound bed, assisting hemostasis, and promoting dermal fibroblasts adhesion, spreading and proliferation. While our scaffold shows less than ideal pore size for typical cellular migration into the bulk of the scaffold, additional work will be necessary to optimize and thus increase pore size to further support cellular scaffold infiltration. We do however show that the overall scaffold porosity for the POC:PAA scaffolds indicates interconnected pores, a necessary parameter to further support cellular migration and infiltration into the bulk of the scaffold.

A key chemical requirement for a wound healing scaffold is hydrophilicity, and the ability to uptake significant amounts of water and wound exudate as well as keep the wound bed moist is essential for wound healing [27, 28]. Our data shows the selected weight ratios of POC:PAA have a hydrophilic contact angle and a high capacity for water absorption, which gives them properties appropriate for water and biological fluid absorption and the ability to maintain a moist environment for wound bed healing [22]. The high surface area to volume ratio of the nanofibrous network also promotes water and wound exudate retention in the wound bed [28]. The water absorption of electrospun polymeric fibers has been reported to range from 17.9%–213%, depending on the material system [22]. Interestingly, our composite scaffold is able to absorb four times more water than most typical electrospun constructs. The high water uptake capabilities of hydrogels have established them as promising wound dressing material because the high water content allows the dressing to cleanse dry, sloughy, or necrotic wounds by rehydration [27]. Hydrogels also encourage autolytic debridement, are non-reactive and non-irritating to biological tissues, which is favorable for wound repair [27]. The properties of the POC:PAA scaffold are tunable and allow it to have similar characteristic potential of hydrogels for wound dressings. There is potential for the electrospun POC:PAA system to be used at all four levels of the wound healing process (bleeding, inflammatory, proliferation, and remodeling). This nanofibrous structure also has the potential to provide cells with needed structural cues for growth and proliferation due to the electrospun fiber's similarities to native ECM. ATR-FTIR was used for chemical corroboration of the scaffolds' hydrophilicity and crosslinking. FTIR confirmed the increase of ester groups, indicating crosslinking, as well as the presence of the hydrophilic functional groups (hydroxyl, carbonyl, carboxyl, and ester) which give the scaffold its hydrophilic character. The presence of the acidic functional groups in POC has been linked to some inherent antibacterial activity [14]. With the inclusion of PAA to the composite scaffold additional acidic groups are present in the polymer. This data was corroborated by the antibacterial tests performed with the POC:PAA scaffolds. The scaffolds were able to kill and inhibit the growth of *S. aureus* and *E. coli*. This showed the scaffold has functional antibacterial capabilities.

As we develop advanced materials to study wound healing, it becomes critical to evaluate the functional capabilities of an engineered scaffold to activate remodeling processes and promote tissue regeneration. It has been established that the introduction of growth factors in the healing cascade can initiate, promote, and accelerate wound healing [9, 17, 29]. Efforts have been made to incorporate growth factors into synthetic scaffolds for sustained and controlled release, such as, core–shell electrospinning [29] and nanoparticle encapsulation [9]. However, these strategies are significantly more complex than the adsorption method we describe and can result in the deactivation of the growth factor [30]. In this study, we report the release of PDGF-$\beta\beta$ by the electrospun POC:PAA scaffolds. This growth factor was selected because it is present in the wound bed during healthy wound healing, and has been shown to promote cellular migration and proliferation. We demonstrated the ability of the scaffold to adsorb and release PDGF-$\beta\beta$ for up to 7 d. *In vivo,* during the wound healing process, the majority of fibroblast recruitment occurs within the first 3 d [31]. We demonstrated the scaffold has the ability to release biologically active PDGF-$\beta\beta$, which could have a therapeutic effect in the days subsequent to surgical debridement or trauma, therefore the POC:PAA scaffolds should create a chemical gradient, promoting chemotaxis of the native dermal fibroblasts into the wound bed. Not only was the concentration of PDGF-$\beta\beta$ released from the POC:PAA scaffolds within the concentration shown to promote fibroblast proliferation (0.6 ng ml^{-1}), but also some degree of biological activity of the growth factor subsequent to processing was confirmed via scratch migration assay. While promising, work still remains to characterize the scaffolds release of other relevant growth factors, or multiple growth factors, and how this function will change *in vivo*. Further, a more in depth characterization and optimization of growth factor loaded and subsequent released is warranted.

Finally, we assessed the biocompatibility of the scaffolds through adhesion, cytotoxicity, and proliferation using D551 skin fibroblasts. We show that the POC:PAA scaffolds can support cell attachment and spreading, as well as the formation of cellular sheets. Additionally, there was evidence of the cells beginning to migrate under the upper layers of the electrospun fibers. This shows that the scaffolds act as a good base for attachment and growth of cells for wound site regeneration. The results from the cytotoxicity assay demonstrated, that neither the 50:50 nor 60:40 scaffolds posed an acute cytotoxic risk to the D551 fibroblasts. In addition to confirming the cytocompatibility of the scaffolds, the ability of the skin fibroblasts to proliferate was also measured. The fibroblasts showed significant increase in metabolic activity via MTT production which was then correlated to cell number. At 7 d, while the rate of proliferation seemed to decrease slightly, we still saw positive cell proliferation as the cells became confluent. Our results were consistent with results seen in the literature, whereby the toxicity of clinically used wound dressings to skin specific cell types was performed over 3 and 7 d [32]. Of particular interest were the results of the proliferation of skin specific cell types, fibroblast, and keratinocytes. In the most successful materials, the results indicate that fibroblast cells showed a population increase of 90%–120% relative to the TCP control after 3 d and this remained consistent after 7 d [32]. The POC:PAA scaffolds showed a 970% population increase for the 50:50 scaffolds and a 1283% increase for the 60:40 scaffolds. Indicating the strong potential of the POC:PAA scaffold to support a robust cellular proliferative response when compared to clinically used wound dressings. In the context of tissue regeneration, this preliminary biocompatibility validation indicates these scaffolds are a promising substrate for cell growth and proliferation. Long term culture studies will be necessary to evaluate the deposition of ECM over time and the reconstruction of tissue.

Recent work in the area of wound healing has investigated other electrospun material systems for wound regeneration, such as Chong *et al* who electrospun PCL and gelatin. Similar to our study, they investigated the biocompatibility of their scaffolds with neonatal human dermal fibroblasts and saw approximately a threefold increase in cell number on their constructs after a week of culture [5]. Relative to this material, the POC:PAA had a greater increase in proliferation of 10 and 7 fold. In addition to fabricating the constructs with synthetic materials, there has been significant use of natural materials like chitosan [7–9]. A study by Xie *et al* was of interest because they incorporated growth factors into their scaffolds in an encapsulated and soluble form. Their release data experienced similar trends with an initial burst release, however, between 72 and 168 h, there was almost no release [9]. Comparatively, the POC:PAA scaffolds exhibited sustained and continued release of PDGF-$\beta\beta$ over 168 h. Overall this indicates the POC:PAA scaffold has significant promise for wound healing applications compared to other constructs currently being developed.

5. Conclusions

Two electrospun nanofibrous scaffolds were successfully fabricated from a novel composite system of POC and PAA. Upon characterization of the scaffold, we were able to achieve: morphological and structural characteristics consistent with properties needed for wound healing applications. In addition to achieving a structural geometry that mimics the native dermal layer, we were also able to demonstrate cellular adherence and proliferation with low acute cytotoxicity to skin fibroblasts. Finally, we were able to show the functionality of the scaffold to deliver a growth factor over a sustained period of time. In conclusion, we were able to develop and characterize a novel biocompatible and biodegradable polymer system that has potential for future wound regeneration applications. Future long term *in vitro* and *in vivo* studies will be necessary to more thoroughly assess the effect of the scaffold on open wound regeneration.

Acknowledgments

The authors would also like to acknowledge Dr Nancy Ruzycki for assistance in obtaining the SEM images used in this study. The authors would also like to thank Phillip Mackie and Sebastian Deleon for experimental assistance.

References

[1] Sen C K *et al* 2009 Human skin wounds: a major snowballing threat to public health and economy *Wound Repair Regen.* **17** 763–71
[2] Center for Disease Control and Prevention 2016 *National and State Healthcare-Associated Infections Progress Report*
[3] Harding K G, Morris H L and Patel G K 2002 Science, medicine, and the future: healing chronic wounds *Br. Med. J.* **19** 160–3
[4] Nae Gyune R, Choongsoo S S and Heungsoo S 2013 Current approaches to electrospun nanofibers for tissue engineering *Biomed. Mater.* **8** 014102
[5] Chong E J *et al* 2007 Evaluation of electrospun PCL/gelatin nanofibrous scaffold for wound healing and layered dermal reconstitution *Acta Biomater.* **3** 321–30
[6] Noh H K *et al* 2006 Electrospinning of chitin nanofibers: degradation behavior and cellular response to normal human keratinocytes and fibroblasts *Biomaterials* **27** 3934–44
[7] Zhou Y *et al* 2008 Electrospun water-soluble carboxyethyl chitosan/poly (vinyl alcohol) nanofibrous membrane as potential wound dressing for skin regeneration *Biomacromolecules* **9** 349–54
[8] Dai T *et al* 2011 Chitosan preparations for wounds and burns: antimicrobial and wound-healing effects *J. Exp. Rev. Anti-infect. Ther.* **9** 857–79
[9] Xie Z *et al* 2013 Dual growth factor releasing multi-functional nanofibers for wound healing *Acta Biomater.* **9** 9351–9

[10] Aytimur A and Uslu İ 2014 Promising materials for wound dressing: PVA/PAA/PVP electrospun nanofibers *Polym. Plast. Technol. Eng.* **53** 655–60
[11] Motlagh D *et al* 2007 Hemocompatibility evaluation of poly (diol citrate) *in vitro* for vascular tissue engineering *J. Biomed. Mater. Res.* A **81** 771–80
[12] Kibbe M R *et al* 2010 Citric acid-based elastomers provide a biocompatible interface for vascular grafts *J. Biomed. Mater. Res.* A **93** 314–24
[13] Hidalgo-Bastida L A *et al* 2007 Cell adhesion and mechanical properties of a flexible scaffold for cardiac tissue engineering *Acta Biomater.* **3** 457–62
[14] Zeimaran E *et al* 2016 Antibacterial properties of poly (octanediol citrate)/gallium-containing bioglass composite scaffolds *J. Mater. Sci., Mater. Med.* **27** 1–11
[15] Su L-C *et al* 2014 Study on the antimicrobial properties of citrate-based biodegradable polymers *Frontiers Bioeng. Biotechnol.* **2** 23
[16] Elliott J E *et al* 2004 Structure and swelling of poly(acrylic acid) hydrogels: effect of pH, ionic strength, and dilution on the crosslinked polymer structure *Polymer* **45** 1503–10
[17] Boateng J S *et al* 2007 Wound healing dressings and drug delivery systems: a review *J. Pharm. Sci.* **97** 2892–923
[18] Demidova-Rice T N, Hamblin M R and Herman I M 2013 Acute and impaired wound healing: pathophysiology and current methods for drug delivery: I. Normal and chronic wounds: biology, cuases, and approaches to care *Adv. Skin Wound Care* **25** 304–14
[19] Yang J, Webb A R and Ameer G A 2004 Novel citric acid-based biodegradable elastomers for tissue engineering *Adv. Mater.* **16** 511–6
[20] Romainor A N B *et al* 2014 Preparation and characterization of chitosan nanoparticles-doped cellulose films with antimicrobial property *J. Nanomater.* **2014** 1–10
[21] Yang J *et al* 2002 Fabrication and surface modification of macroporous poly (L-lactic acid) and poly (L-lactic-co-glycolic acid) (70/30) cell scaffolds for human skin fibroblast cell culture *J. Biomed. Mater. Res.* A **62** 438–46
[22] Zahedi P *et al* 2009 A review on wound dressings with an emphasis on electrospun nanofibrous polymeric bandages *Polym. Adv. Technol.* **21** 66–95
[23] Abrigo M, McArthur S L and Kingshott P 2014 Electrospun nanofibers as dressings for chronic wound care: advances, challenges, and future prospects *Macromol. Biosci.* **14** 772–92
[24] Boland C P 2008 Nanofiber technology: designing the next generation of tissue engineering scaffolds *Adv. Drug Deliv. Rev.* **59** 1413–33
[25] Kumbar S G *et al* 2008 Electrospun poly(lactic acid-co-glycolic acid) scaffolds for skin tissue engineering *Biomaterials* **29** 4100–7
[26] Chen M *et al* 2007 Role of fiber diameter in adhesion and proliferation of NIH 3T3 fibroblast on electrospun polycaprolactone scaffolds *Tissue Eng.* **13** 579–87
[27] Chaby G *et al* 2007 Dressings for acute and chronic wounds *Arch. Dermatol. Res.* **143** 1297–304
[28] Boateng J S *et al* 2008 Wound healing dressings and drug delivery systems: a review *J. Pharm. Sci.* **97** 2892–923
[29] Yang Y *et al* 2011 Promotion of skin regeneration in diabetic rats by electrospun core-sheath fibers loaded with basic fibroblast growth factor *Biomaterials* **32** 4243–54
[30] Ji W *et al* 2011 Bioactive electrospun scaffolds delivering growth factors and genes for tissue engineering applications *Pharm. Res.* **6** 1259–72
[31] Velnar T, Bailey T and Smrkolj V 2009 The wound healing process: an overview of the cellular and molecular mechanisms *J. Int. Med. Res.* **37** 1528–42
[32] Dover R *et al* 1995 Toxicity testing of wound dressing materials *in vitro Br. J. Plast. Surg.* **48** 230–5